Helmholtz-Zentrum Dresden-Rossendorf (HZDR)

HZDR
HELMHOLTZ ZENTRUM
DRESDEN ROSSENDORF

Supported Two-Dimensional Materials under Ion Irradiation: the Substrate Governs Defect Production

Kretschmer, S.; Maslov, M.; Ghaderzadeh, S.; Ghorbani-Asl, M.; Hlawacek, G.; Krasheninnikov, A. V.;

Originally published:

August 2018

ACS Applied Materials and Interfaces 10(2018)36, 30827-30836

DOI: https://doi.org/10.1021/acsami.8b08471

Perma-Link to Publication Repository of HZDR:

https://www.hzdr.de/publications/Publ-27447

Release of the secondary publication
on the basis of the German Copyright Law § 38 Section 4.

Supported Two-Dimensional Materials under Ion Irradiation: the Substrate Governs Defect Production

Silvan Kretschmer,[*,†] Mikhail Maslov,[†,‡] Sadegh Ghaderzadeh,[†] Mahdi Ghorbani-Asl,[†] Gregor Hlawacek,[†] and Arkady V. Krasheninnikov[†,¶]

Institute of Ion Beam Physics and Materials Research, Helmholtz-Zentrum Dresden-Rossendorf, 01328 Dresden, Germany, Moscow Institute of Physics and Technology, Dolgoprudny, Russia, and Department of Applied Physics, Aalto University, 00076 Aalto, Finland

E-mail: s.kretschmer@hzdr.de

Abstract

Focused ion beams perfectly suit for patterning two-dimensional (2D) materials, but the optimization of irradiation parameters requires full microscopic understanding of defect production mechanisms. Contrary to free-standing 2D systems, the details of damage creation in supported 2D materials are not fully understood, while the majority of experiments have been carried out for 2D targets deposited on substrates. Here we suggest a universal and computationally efficient scheme to model the irradiation of supported 2D materials, which combines analytical potential molecular dynamics with Monte Carlo (MC) simulations, which makes it possible to assess independently the contributions to the damage from backscattered ions and

[*]To whom correspondence should be addressed

[†]Institute of Ion Beam Physics and Materials Research, Helmholtz-Zentrum Dresden-Rossendorf, 01328 Dresden, Germany

[‡]Moscow Institute of Physics and Technology, Dolgoprudny, Russia

[¶]Department of Applied Physics, Aalto University, 00076 Aalto, Finland

atoms sputtered from the substrate. Using the scheme, we study defect production in graphene and MoS_2 sheets, which are the two most important and wide-spread 2D materials, deposited on a SiO_2 substrate. For helium and neon ions with a wide range of initial ion energies including those used in commercial helium ion microscope (HIM), we demonstrate that depending on ion energy and mass, defect production in 2D systems can be dominated by backscattered ions and sputtered substrate atoms rather than by the direct ion impacts, and that the amount of damage in 2D materials heavily depends on whether a substrate is present or not. We also study the factors which limit the spatial resolution of the patterning process. Our results, which agree well with the available experimental data, provide not only insights into defect production, but also quantitative information, which can be used for the minimization of damage during imaging in HIM or optimization of the patterning process.

Introduction

Ion irradiation[1,2] is one of the most powerful tools to change the atomic structure and properties of the materials through controllable introduction of impurities and defects. The technique suits particularly well for the processing of two-dimensional (2D) materials, because due to the small thickness of the system a uniform distribution of dopants and defects with regard to their depth is not an issue, as evident from numerous examples for graphene[3–9] or transition metal dichalcogenides (TMDs).[10–16] Moreover, exposure to energetic ions can be combined with in-situ or post-irradiation chemical treatment of these atomically thin targets[11,17–21] to incorporate foreign atoms into the atomic network due to chemically reactive vacancies.

Focused ion beams can be used to produce defects with a high spatial resolution. They can also be employed for cutting and patterning 2D materials.[22] In this context, the He-ion microscope (HIM),[23] where He or Ne ion beams have sub-nanometer diameters, have been demonstrated to be a perfect tool for not only getting insights into sample morphology, but also altering its structure and geometry at the nano-scale. Specifically, structural defects were controllably introduced in a few-layer MoS_2 sample[15] so that its stoichiometry and electronic transport properties could be

tuned. Nanoribbons with widths as small as 1 nm were reproducibly fabricated in graphene[4,6,9,24] and MoS_2 sheets.[15] An increase in Young's modulus of $MoSe_2$ samples irradiated in HIM was reported, along with the possibility to tune optical properties of TMDs.[25] Structural changes in free standing graphene and that encapsulated between sheets of hexagonal boron nitride under focused helium ion beam irradiation have been studied[26] in the HIM and showed the benefits of graphene encapsulation for post-synthesis doping and self-healing of the beam-induced lattice damage.

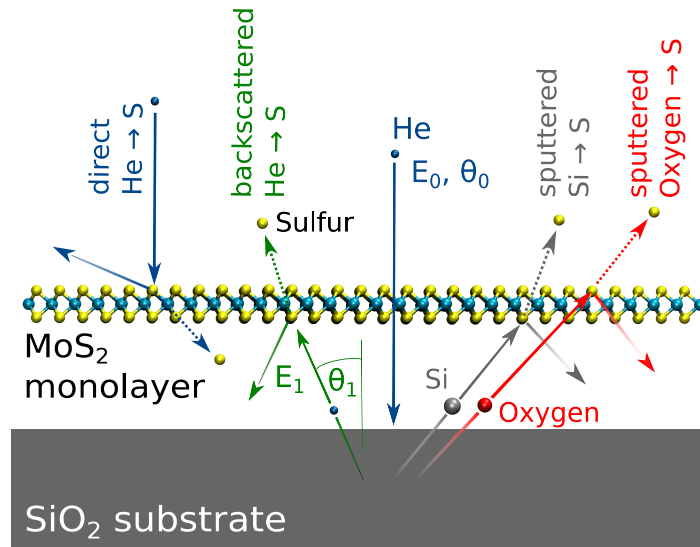

Figure 1: Schematic presentation of the channels for defect production in a supported 2D material under ion irradiation by the example of He ion impacts on a MoS_2 sheet on a SiO_2 substrate. Defects, e.g, S vacancies, can be produced by direct ion impacts, by backscattered ions and atoms sputtered from the substrate.

In the typical experimental setup used for ion bombardment, the 2D target is placed on a substrate, normally a Si/SiO_2 slab. However, the experimental data is frequently rationalized using atomistic computer simulations carried out for free-standing systems.[27–30] It is tacitly assumed that most of the defects are produced from direct interaction of the primary beam with the target, which as we show below, is not generally true, especially for the case of light ion irradiation in the HIM. Indeed, the experiments carried out for supported and free-standing 2D MoS_2[31] and graphene[32] clearly indicate that there are substantial differences in the amount of the beam-induced damage and the properties of the irradiated samples.

Contrary to free-standing targets (e.g., graphene[33] or MoS_2 suspended on a TEM grid[15,31]), where all the defects are created by the impinging ions, the substrate can affect defect production in several ways. Putting aside the case of highly-charged ions[34] and swift heavy ions which literally 'blow-up' the substrate so that the 2D material on top is torn apart by the atoms coming from the substrate,[35] defects in the 2D system can be produced at moderate ion energies by two other mechanisms, in addition to (i) direct ion impacts: (ii) backscattered ions [1] and (iii) atoms sputtered from the substrate, as schematically illustrated in Fig. 1. The latter two mechanisms are indirect defect production channels. Moreover, experimental investigations[9,32,36–38] using state of the art focused ion beam technology indicate that the substrate hinders higher patterning resolutions, so that a detailed microscopic understanding of the role of the substrate and its effects on defect production under ion irradiation is required. The substrate also plays the key role in the evolution and annealing of defects.[39] Several attempts to account for the effects of the substrate have been carried out for high-energy (MeV) heavy ion[40] and 30 keV He[32] ion irradiation of supported graphene, but the trends and physical processes involved were not systematically analyzed. Computationally, this is a very challenging task, as first-principles approaches cannot be used due to the high computational costs required to collect representative statistics for systems composed from a few thousand atoms. Furthermore, analytical potentials developed for multi-atomic systems are either of limited accuracy or are still computationally too expensive for adequate modeling of the system.

In this work, we suggest an efficient scheme to model the irradiation of supported 2D materials, which combines analytical potential molecular dynamics (MD) simulations for the 2D material, augmented with a universal repulsive potential to account for the effects of the substrate on sputtered atoms and a Monte Carlo (MC) method. This allows to assess independently the contributions to the damage from backscattered ions and atoms sputtered from the substrate and hitting the supported 2D system. Using the scheme, we study defect production in graphene and MoS_2

[1]The charge state of the projectile cannot be accounted for in the classical MD simulations. However, in order to differentiate between target/substrate atoms and primary projectiles, we refer to the former as 'atoms' and the latter as 'ions', even though their charge state is unknown.

sheets, which are the two most widely used 2D materials, deposited on a SiO_2 substrate. We pay particular attention to helium and neon ions since they are used in HIMs for material modification, nano-patterning and imaging purposes.[23] While for the patterning processes the controllable production of defects in a narrow region is desirable, minimal defect production should be aimed at for non-destructive imaging. Using our approach, we access defect production rates of He, Ne and Ar ions for a wide range of initial ion energies including the HIM-typical energy interval from 1 keV to 30 keV. Our results indicate that in this energy interval defect production in graphene and MoS_2 is dominated by backscattered ions and sputtered substrate atoms rather than by the direct ion impacts. Consequently the area in which defects are introduced is dramatically enlarged as compared to the free-standing irradiated material, and in the case of HIM based irradiation, to the beam diameter (typically 0.5 nm and 1.8 nm for He and Ne, respectively).

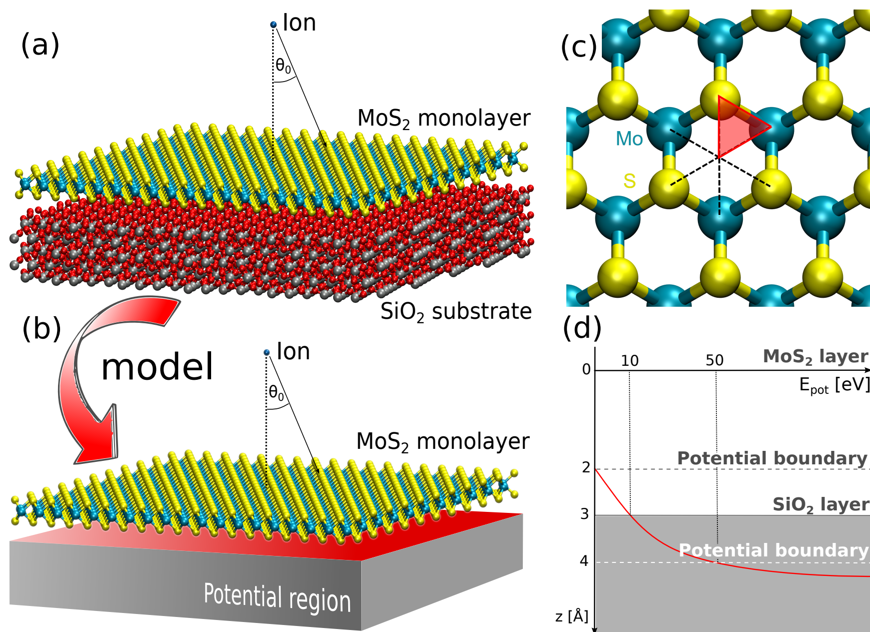

Figure 2: Simulation setup. (a) Atomistic model of MoS_2 on a SiO_2 substrate. (b) The corresponding system where the substrate is modelled using an external potential. (c) Definition of minimal irreducible area used for choosing the ion impact points. (d) External potential acting on the atoms of the 2D target. The MoS_2 is positioned at zero z coordinate.

Results and Discussion

He ion irradiation. MD and MC simulations of impacts of the projectiles (He, Ne, Ar ions as well as Si and O atoms) onto 2D materials (graphene and monolayer MoS_2) were carried out as described in detail in the Methods section. As we are aiming at assessing the effects of low-dose irradiation, we assumed that the ions always impinge into pristine material. To collect representative statistics for different impact points, an irreducible area was chosen as depicted in Fig. 2(c). In order to include the effects of the SiO_2 substrate in the MD simulations and at the same time have a computationally efficient scheme, we modelled the substrate as an external potential acting on the atoms in the corresponding region (see Figure 2). The potential has no effect on the impinging ions, while backscattered ions were treated using a statistical approach with the data collected from the MC simulations. Splitting defect production into two different channels is possible due to a very small probability for the backscattered ions and sputtered atoms to hit the area where defects were already produced by that same ion. Due to the geometry of the system, we independently considered defect production by the ions coming from *above* the 2D target, with ion velocity vectors pointing towards the substrate (direct impacts), and from *below*, with ion velocity vectors pointing away from the substrate (the case for backscattered ions and sputtered substrate atoms).

The average number of defects produced by impinging and backscattered particles, along with those produced by sputtered substrate atoms, were obtained from MD simulations as functions of ion energy and angle. The results for He ions are presented in Fig. 3. It is evident that the number of sputtered S and C atoms increases with ion energy, then quickly drops due to a decrease in the cross-section to displace an atom from the 2D target. This is in agreement with the results of previous calculations.[27,28] The atoms sputtered from the substrate are more abundant than backscattered ions for typical HIM energies. Detailed statistics data of projectile characteristics obtained from the MC data, such as energy and angle probability distributions, can be found in the supplemental material in Fig. 11. The number of sputtered atoms depends also on the incidence angle, with the maximum in defect production being shifted towards higher ion energies for off-normal incidence.

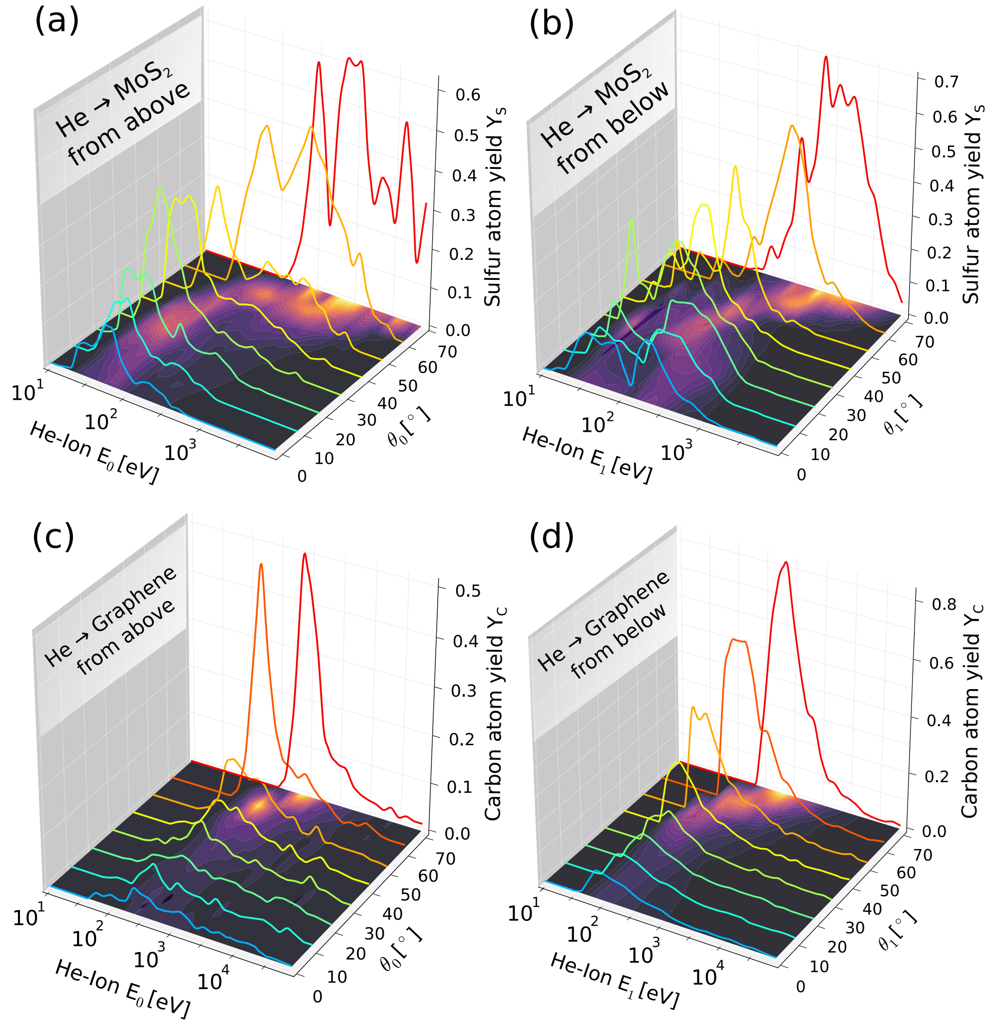

Figure 3: Number of atoms sputtered from supported monolayer MoS_2 and graphene by energetic He ions as obtained from molecular dynamic simulation. Impacts of He atoms onto MoS_2 from above (a) and below (b). Impacts of He atoms into graphene from above (c) and below (d).

We performed similar MD calculations for the impacts of O and Si projectiles onto MoS_2 and graphene sheets. Only impacts from 'below' were considered. The results are presented in Fig. 4. The production of defects shows similar trends as for He ions, but the number of sputtered atoms is considerably higher due to larger atomic masses of O and Si atoms as compared to He.

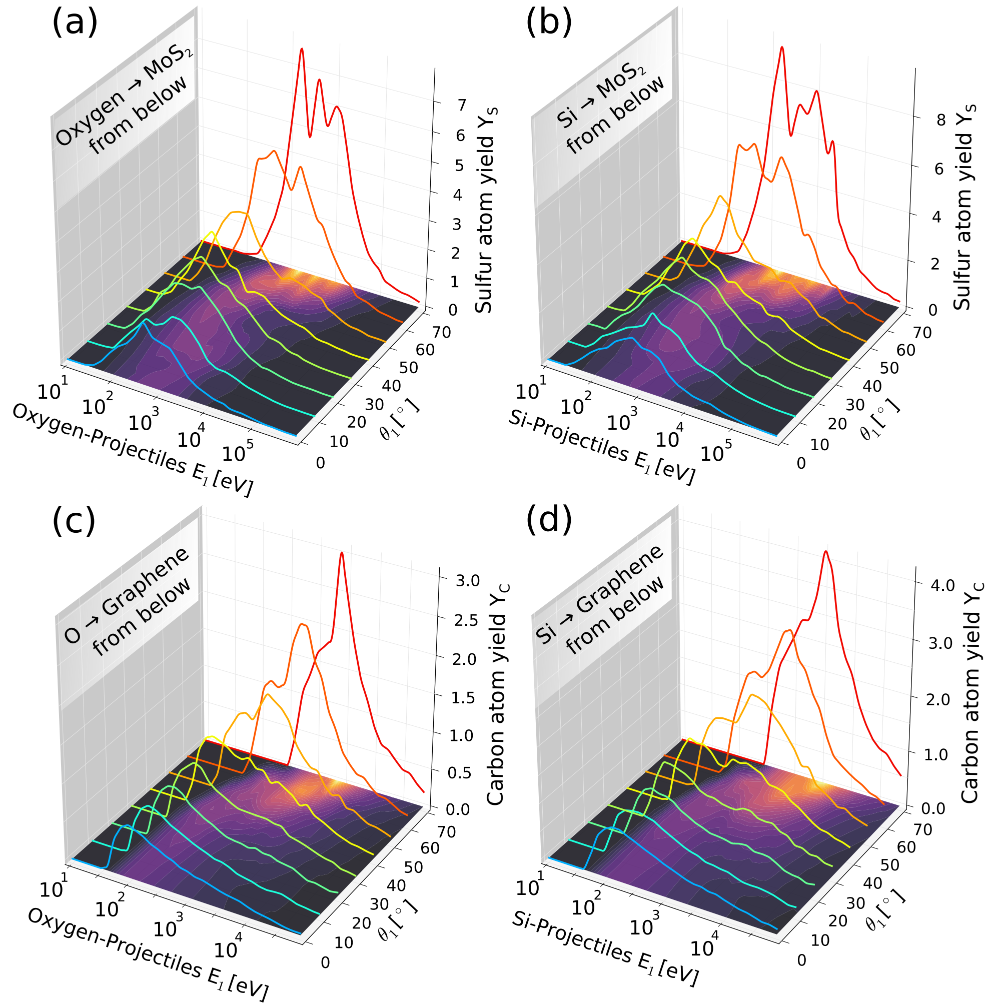

Figure 4: Number of atoms sputtered from supported monolayer MoS_2 and graphene by O and Si projectiles hitting the sheets from below as obtained from molecular dynamic simulation. Impacts of O (a) and Si (b) projectiles onto MoS_2. Impacts of O (c) and Si (d) projectiles onto graphene.

Based on the calculated number of atoms sputtered from MoS_2 and graphene sheets per single impact of He, O and Si projectiles, we evaluated the average number of defects produced in the system by He ion irradiation. To match the usual experimental geometry, normal incidence of He ions was assumed. Using the MC approach, we obtained the number of backscattered He ions as well as sputtered O and Si atoms from the substrate as functions of initial energy of He ions. Using MD simulations we also assessed the number of ions which have passed through the sheet, which is different from unity at energies below 1 keV. The results for MoS_2 sheet are shown in Fig. 5.

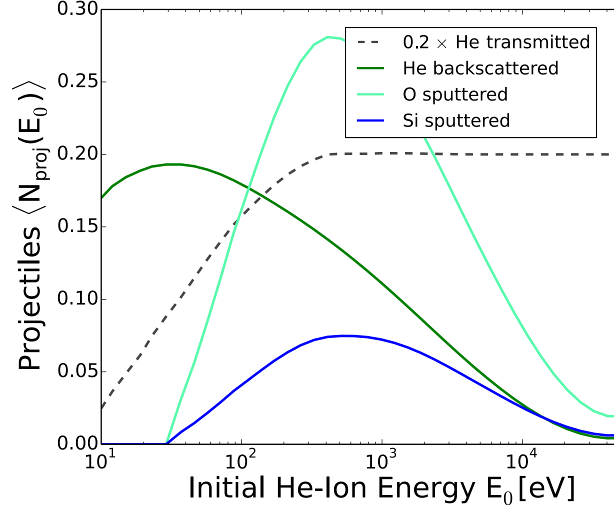

Figure 5: Number of He ions which have passed through MoS_2 sheet, the number of ions backscattered by SiO_2 substrate, along with the number of sputtered O and Si atoms as functions of initial He ion energy as obtained from MC calculations. Note that for better visualization the transmission probability of He ions through monolayer MoS_2 is scaled by a factor of 0.2.

By combining the MD and MC data, the average number of sputtered target atoms $\langle N_{\text{total}} \rangle$ (Mo, S for MoS_2 and C for graphene) can now be calculated:

$$\langle N_{\text{total}} \rangle = \langle N_{\text{direct}}(\text{He}) \rangle + \langle N_{\text{BS}}(\text{He}) \rangle + \langle N_{\text{SP}}(\text{Si}, \text{O}) \rangle \tag{1}$$

where $\langle N_{\text{direct}}(\text{He}) \rangle$ is the averaged number of directly sputtered atoms per He-ion and $\langle N_{\text{BS}}(\text{He}) \rangle$, $\langle N_{\text{SP}}(\text{Si}, \text{O}) \rangle$ are the contributions from the backscattered ions and sputtered substrate atoms, respectively. The average number of created S-vacancies from direct impacts is given by $\langle N_{\text{direct}} \rangle = \langle N_{\text{above}}(E_0, \theta_0 = 0) \rangle$, where $\langle N_{\text{above}} \rangle$ is derived from MD simulations with impacting ion starting in the upper half plane with velocity pointing towards the substrate (see the blue trajectory in Fig. 1). The average number of S-vacancies created by backscattered ions $\langle N_{\text{BS}}(E_0) \rangle$ in turn is estimated by averaging over all possible trajectories (defined by energies and angles E_1, θ_1) of the backscattered ions. This is realized by performing the probability distribution weighted integration of the average number of defects $\langle N_{\text{below}}(E_1, \theta_1) \rangle$ (see green trajectory in Fig. 1) over the energies and angles of the backscattered particles. The integral is further multiplied by the probability $P_{\text{BS}}(E_0)$

for the ion to be backscattered and hit the 2D target again and the transmission probability $T(E_0)$ to obtain the average number of sputtered S atoms

$$\langle N_{\mathrm{BS}}(E_0)\rangle = T(E_0)\cdot P_{\mathrm{BS}}(E_0)\cdot \int \mathrm{d}E_1\, p_{\mathrm{BS}}(E_1|E_0)\cdot \int \mathrm{d}\theta_1\, p_{\mathrm{BS}}(\theta_1)\langle N_{\mathrm{below}}(E_1,\theta_1)\rangle, \qquad (2)$$

where $p_{\mathrm{BS}}(\theta_1)$ and $p_{\mathrm{BS}}(E_1|E_0)$ are the angular and energy probability distribution of the backscattered ions, respectively. The latter depends on the incident ion energy E_0 while the former is universal.

A similar expression can be used to evaluate the effects of sputtered atoms $\langle N_{\mathrm{SP}}(E_0)\rangle$ on vacancy production with the backscattering probability replaced by the average number of sputtered atoms and summing over the contributions from Si and O atoms (grey and red trajectories in Fig. 1).

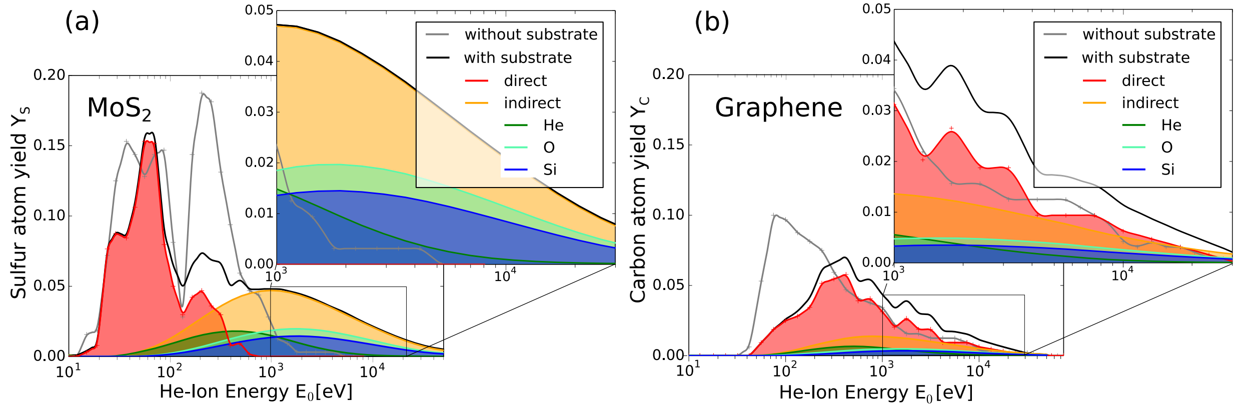

Figure 6: Average number of atoms sputtered from MoS_2 (a) and graphene (b) per He ion impact. The corresponding numbers for free-standing monolayers (grey) and the direct sputtering (red) are shown for comparison. The insets magnifies for the range of ion energies from 1 keV to 30 keV He used in HIM.

The results obtained with the combined MD and MC approach are presented in Fig. 6. The data for damage production by direct impacts and the data for free-standing material are obtained directly from MD simulations carried out for the same setup. The results for free-standing systems agree well with the previously published data.[27,28] As for MoS_2, the average number of sputtered S-atoms for He irradiation without substrate shows two pronounced peaks which can be attributed to the sputtering from the top and bottom sulfur layers.[27] The data for direct He ion impacts also

shows two peaks, but the second one is considerably suppressed, meaning that the substrate reduces the forward sputtering for the second layer. This is supported by the averaged number of sulfur vacancies per layer obtained by analyzing the defect density and locations after the ion impact (Wigner-Seitz analysis of the final configurations of the MD data).

As compared to the free-standing system, the direct defect production in supported MoS_2 is smaller in the energy range from 400 eV to 800 eV. This is a consequence of the reduced sputtering from S-layer facing the substrate. S recoils generated there (in forward direction) can not easily leave the sample. Furthermore, for typical HIM energies, see the inset in Fig. 6(a), direct sputtering is almost completely absent, while defect production is still noticeable in the supported system. In this energy range indirect sputtering, more specifically the sputtering by substrate atoms can clearly be identified as the dominant damage mechanism. Oxygen has the largest influence, but Si sputtering appears to be more efficient, as for a smaller number of projectiles a comparable amount of damage (sulfur sputtering) is produced. Within binary collision approximation this can be attributed to a larger momentum transfer for mass ratio closer to unity ($m_{\mathrm{Si}}/m_{\mathrm{S}} = 0.875$, $m_{\mathrm{O}}/m_{\mathrm{S}} = 0.5$). Likewise, the mass ratio of He to Mo atom $m_{\mathrm{Mo}}/m_{\mathrm{He}} = 24$ explains the negligible number of sputtered Mo-atoms found in the combined MC/MD simulations for both direct and indirect sputtering. Fig. 6(b) illustrates defect production in free-standing and supported graphene. It is evident that as in MoS_2, the substrate impedes the production of defects at very low energies, but the effect is stronger than in MoS_2, as graphene has only one layer of atoms. At high ion energies more defects are produced in the supported system with a substantial contribution from sputtered O and Si atoms. The birds eyes view on the defect production mechanisms of He irradiated MoS_2 reveals that the substrate has a dramatic influence on the atom sputtering rate. For MoS_2, the sputtering rate is approximately five times larger than without substrate in the HIM energy interval. A similar behavior is observed for graphene. Such an increase in the damage rate was also found experimentally for the He ion bombarded of graphene supported by a SiO_2/Si substrate.[32]

Ne ion and Ar ion irradiation. Similar to the modeling of He ion irradiation, we carried out simulations of the impacts of heavier Ne and Ar ions onto a supported MoS_2 sheet. We found that

the number of backscattered ions decreases dramatically as compared to helium, while the average number of sputtered substrate atoms increases, see Fig. 7. In particular, the probability for Ne ions to be backscattered from the SiO_2 substrate is less than 1% for all the energies and is zero for Ar. Both observations can be understood within binary collision approximation considering the projectile-to-target mass ratio, as backscattering is more likely for lighter ions and the momentum transfer to secondary projectiles is more efficient for a mass ratio close to unity ($m_{\text{He}}/m_{\text{Si}} = 0.14$, $m_{\text{Ne}}/m_{\text{Si}} = 0.71$, $m_{\text{Ar}}/m_{\text{Si}} = 1.42$). As expected, for increasing ion mass the maximum of the sputtering yield shifts to higher energies.

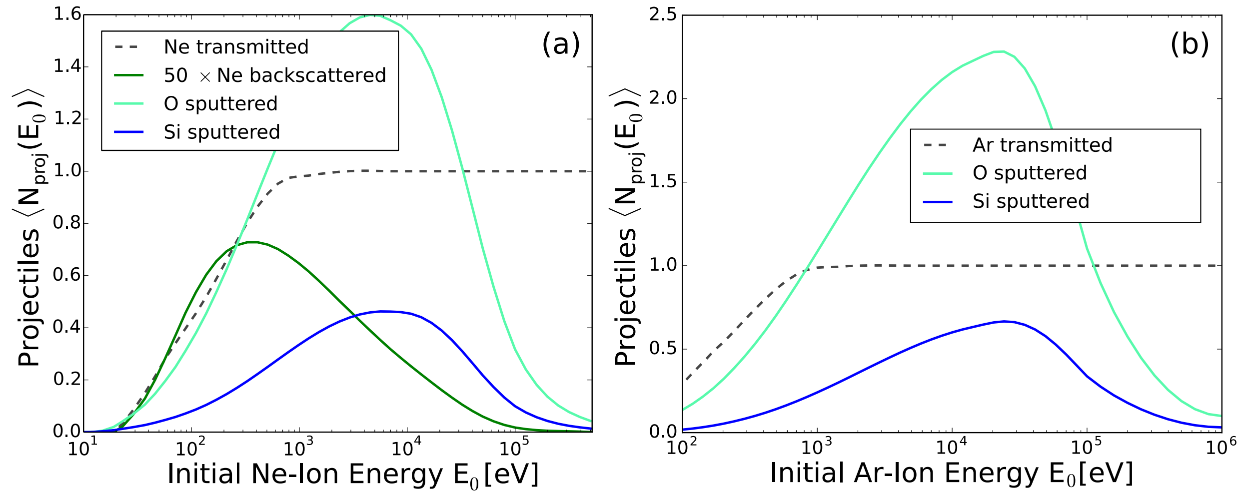

Figure 7: Transmitted and back scattered ions along with the sputtered substrate atoms as functions of ion energies for neon (a) and argon (b). Note that the average number of backscattered ions for Ne is scaled by factor of 50.

Fig. 8 illustrates the effects of the substrate on the defect production for MoS_2 and graphene. The results for free-standing monolayers are also presented for the sake of comparison. The data for free-standing monolayers, shown as a reference, agrees well with previously published results for noble gas ion bombarded MoS_2 and graphene.[27,28] As follows from the data on the abundance of the available projectiles, Fig. 7, the contribution to the damage in the 2D target from backscattered particles is negligible, and defect production process is governed by direct impacts of ions and by atoms sputtered from the substrate.

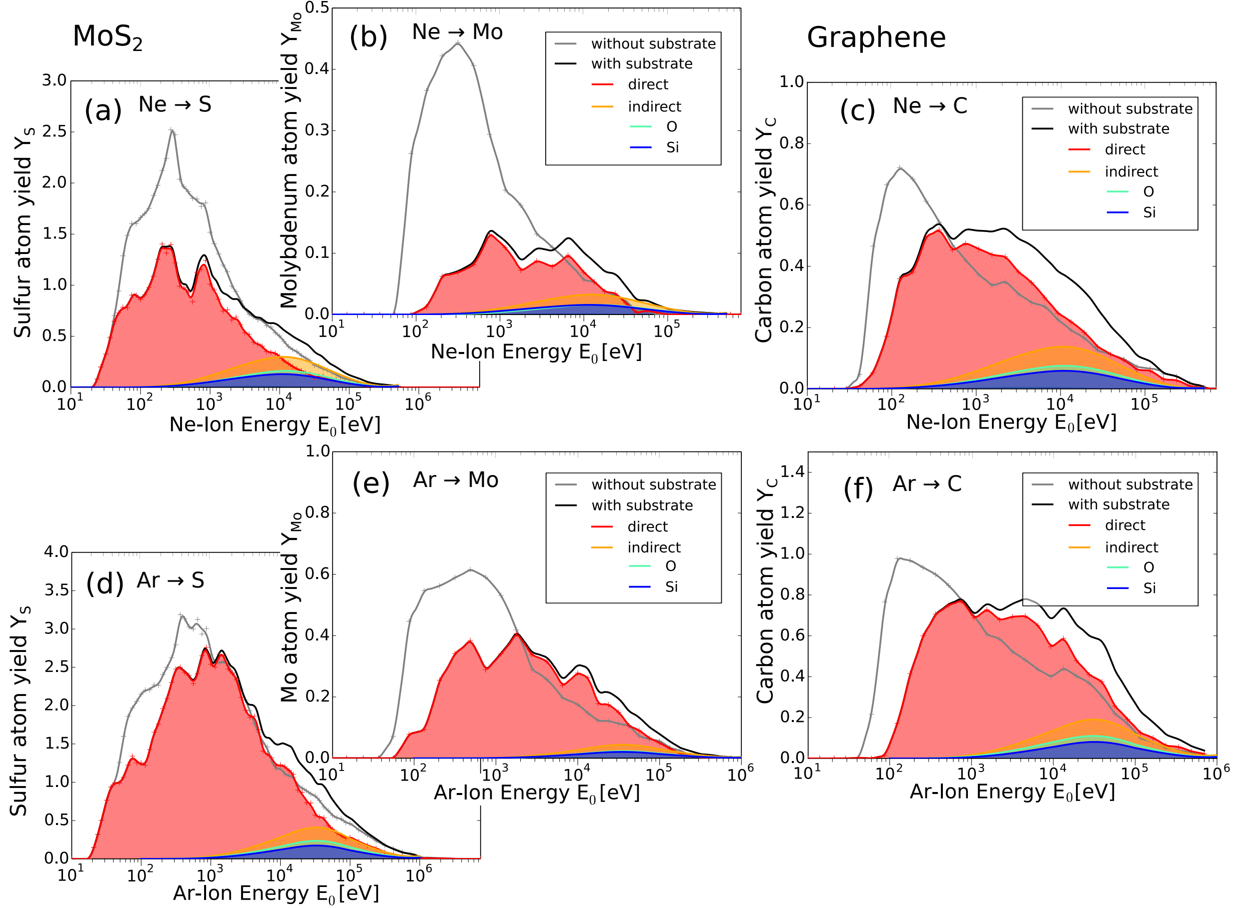

Figure 8: Average number of sputtered atoms from MoS_2 (left) and graphene (right panels) for Ne (a-c) and Ar (d-f) impacts. The corresponding numbers for free-standing monolayers (grey) are shown for comparison.

A salient feature is the suppression of defect production at low ion energies, as the substrate 'stops' the atoms sputtered away from the target and increases the probability for immediate recombination of the vacancy-interstitial pair. It is also evident from Fig. 8 that while the total sputtering yield increases due to the higher ion mass, the enhancement in the indirect sputtering of target atoms is less pronounced than the boost in direct sputtering. This means that for heavier ions the effect of the substrate on defect production is smaller. Nevertheless, as panels (a-c) in Fig. 8 – illustrating sputtering of S, Mo and C atoms by Ne – demonstrate, the combined effect of direct and indirect sputtering is twice as large as the sputtering yield without substrate in the energy range relevant for HIM (from 1 keV to 30 keV). This indicates that for neon in the HIM the

substrate still plays an important role, while the processes which enhance or diminish sputtering compensate each other in case of argon irradiation, as panels (d-f) in Fig. 8 illustrate. For the latter, a substantial increase in the sputtering yield due to the presence of a substrate cannot be observed.

Spatial distribution of defects with regard to the impact point of the ion. The substrate not only influences the number of defects produced under ion bombardment, but also has an important impact on the spatial distribution of defects. From the application point of view, the spatial extension of the defect region in supported 2D materials is of paramount importance, as it determines the resolution of the HIM during patterning of 2D materials. Our combined MC/MD simulations provide direct access to the spatial distribution of defects with respect to the impact point of the ion. While the impinging ions produce defects only in the immediate vicinity of the impact point (1 nm range; see the inset in panel (c) of Fig. 9), the backscattered ions and atoms sputtered from the substrate give rise to the production of defects in a wider region, with the average extension of the region being dependent on initial energy of He (or Ne) ions.

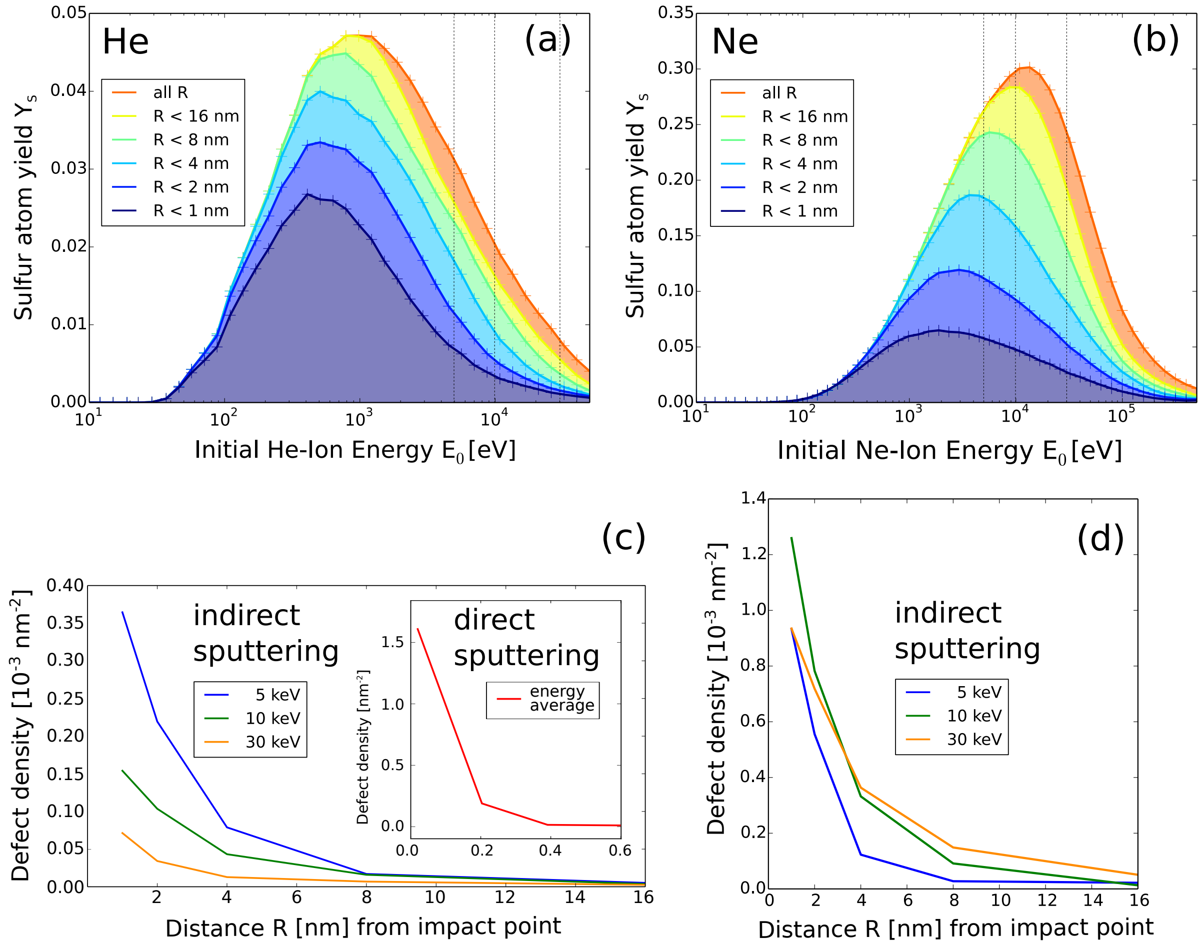

Figure 9: Spatial distribution of defects. Average number of S atom sputtered by backscattered He, Ne ions and Si, O atoms originating from different regions with respect to the impact point. Panel (a) and (b) show the indirect defect production for different radii from the impact point for He and Ne ions, respectively. Panel (c) depicts the defect density for three selected energies taken as cross sections in panel (a) (dashed vertical lines). Defect density with respect to the impact point is compared to that obtained by direct sputtering (inset), showing increased extension of the defect region for indirect sputtering. Panel (d) shows the indirect defect density for neon ions.

F For both He and Ne ions with energies below 1 keV almost all sulfur vacancies are produced within a 8 nm radius from the impact point. However, for typical HIM energies the defective region is more extended: up to two thirds of defects are produced outside the 8 nm region, as is evident from Fig. 9, panels (a) and (b). Although defect density decays rapidly with increasing distance R from the impact point, defects can be created at typical HIM energies even outside the 10 nm range. As compared to the free-standing material, where defects are expected only in the close vicinity of

the impact point, this result agrees well with the previous experimental observations and indicates that backscattered ions and sputtered substrate atoms are the main reason for resolution limitations in patterning of supported 2D materials.[9,36,38] It is interesting to note that spatial extend of the damage also depends on ion mass. As is evident from our results (see Fig. 9) that higher energies (e.g., 30 keV) would give a better spatial resolution for He, while it is the other way around for Ne. For the latter, the lowest energies still attainable in HIM (e.g., 5 keV) are preferable.

Comparison to the experimental results. To validate our approach, we analyzed the available experimental data on the amount of damage produced in supported graphene and MoS_2 under ion irradiation. It should be pointed out that the direct comparison of the theoretical and experimental defect densities is not straightforward. On the one hand, in-situ annealing of defects even at room temperature is possible, and on the other hand, at high irradiation doses more defects can be produced, when defects already exist in the area where the ion hits the sample. Neither of these effects can easily be accounted for in simulations, but one can assume that they cancel each other to the first order. The accurate determination of defect concentrations in the experiments from Raman spectra or EDX data is also a challenge.

Irradiation of free-standing MoS_2 flakes by 30 keV He ions gave rise to the loss of about 50% of the S atoms at a dose of 10^{18} He^+/cm^2, while an order of magnitude smaller dose was required for the sample on a substrate.[15] Our results (Fig. 6) indicate that $Y \sim 0.008$ S atoms are sputtered away by 30 keV He ion. A dose of 10^{17} He^+/cm^2 corresponds to $N_I \sim 90$ ions hitting the primitive cell area. Correspondingly, the relative number of atoms which should still remain in the system is $(2 - Y \cdot N_I)/2 \sim 0.6$, which is in a very good agreement with the experimental data.

As for He ion irradiation of graphene, our simulations indicated that the number of defects should be larger in supported samples (as compared to free-standing) by a factor of about three, which qualitatively agrees with the experimental ratio[32] for doses below 10^{15} He^+/cm^2. Our results for 500 eV Ar irradiation on MoS_2 were also in order-of-magnitude agreement with the dose (about 5×10^{15} Ar^+/cm^2) required to sputter ca. 25% of the S atoms.[19] The agreement with the published experimental values for higher Ar energies is even more striking: while for bilayer graphene on

SiO_2 substrate irradiated with 100 keV argon ions a carbon sputtering yield of 0.25 atoms per ion in the top layer (0.13 due to enhanced annealing in the second layer) is determined in the experiment,[39] our results – not accounting for annealing effects – yield 0.28 carbon atoms per Ar ion. For free-standing system the model suggests only half of this value. Furthermore, our predictions for graphene are consistent with the data extracted by Li et.al.[40] from the Raman spectra of irradiated graphene samples: the sputtering yield in graphene bombarded with 35 keV carbon ions is estimated as 0.150 C atoms per incident ion,[41] which is slightly smaller than our predicted value of 0.22 C atoms per (heavier) neon ion. A similar observation can be made for graphene irradiated with 30 keV N ions (0.186 atoms/ion),[42] which is in line with our simulation results for 30 keV Ne ions (0.25 atoms/ion). In both cases the calculated sputtering yield of C atoms for free-standing graphene samples is much smaller than the experimental value.

Conclusions

We suggested a computationally efficient scheme which combines analytical potential MD and MC simulations to model the irradiation of supported 2D materials. The scheme makes it possible to assess independently the contributions to the damage from backscattered ions and atoms sputtered from the substrate. The approach can in principle be applied to any 2D material/substrate combination, provided that the potential for the 2D target exists. The method does not require to explicit account for the interaction of the substrate material with the target, as the substrate is replaced by an effective repulsive potential. Using this scheme, we studied defect production in graphene and MoS_2 sheets on a SiO_2 substrate. Our results, which agree well with the available experimental data, demonstrate that depending on ion mass and energy the number of defects produced in the target by the impinging ions can be smaller or larger than in the free-standing material, that is deposited on top of a trench in the substrate or on a TEM grid. For helium and neon ions with a wide range of initial ion energies including those used in commercial helium ion microscope, we showed that defect production in 2D systems can be dominated by backscattered ions and sputtered

substrate atoms rather than by the direct ion impacts. The last statement is especially true for light ions. In particular, this is the case for 30 keV He ions, most widely used for imaging and patterning of 2D targets. We also studied the factors which limit the spatial resolution of the patterning process. Our results provide microscopic insights into defect production mechanism, along with the quantitative information, which can be used for the minimization of damage during imaging or optimization of the patterning process.

Methods

Molecular dynamic (MD) simulations were carried out using the LAMMPS[43] package to extract the statistics of defects produced by impacts of the projectiles (He, Ne, Ar ions and Si O atoms) onto the 2D materials (graphene and monolayer MoS_2). The MD calculations of ion impacts onto targets were performed as described previously.[27] At minimum 320 impact points per energy and angle configuration were chosen. A modified Stilinger-Weber (SW) potential[44] with a smooth transition to the Ziegler-Biersack-Littmark (ZBL) potential[45] for small distances was used. For collisions of ions with the target atoms the ZBL part dominates at high energies, so that ZBL potentials were also used to describe impacts of atoms sputtered from the substrate. This approximation is further validated by a rather weak interaction of O and Si adatoms with pristine graphene and MoS_2: the adatoms are mobile on graphene[46] and MoS_2[47] surfaces, so that they should form compounds and desorb from the system. The MD calculations for ion bombardment of graphene were carried out using the combined Tersoff and ZBL potential.

The effects of the SiO_2 substrate were modelled as an external potential acting on the target atoms (Mo,S or C) in the corresponding region (see Fig. 2). The potential in this approximation can be expressed as

$$U(z) = A\left(\mathrm{e}^{\,\beta(z-z_0)} - 1\right), \tag{3}$$

where the coefficients are determined by the boundary of the potential region $z_0 = 2\,\text{Å}$, the surface approximation energy – the energy required to approach a surface located at $d = 3\,\text{Å}$ (distance

from the monolayer)[48] from infinity $U(z = d) = 10\,\text{eV}$, and a defined kinetic energy loss of the incident particle with $U(z = 4\,\text{Å}) = 50\,\text{eV}$. This yields the coefficients $A = 10/3$ eV ≈ 3.33 eV and $\beta = 2\ln 2\,\text{Å}^{-1} \approx 1.38\,\text{Å}^{-1}$.

The MD approach was combined with the Monte Carlo method implemented in the SRIM code[49] to account for projectile properties and their statistics (e.g. backscattering probability, energy and angle distributions). The MD and MC approaches were combined by treating the impacts of the projectiles on the 2D target material in detail with MD (accessing short time and length scale), while the projectiles statistic was sampled according to the results of MC calculations (covering larger time and length scales).

Acknowledgements

We thank S. Facsko for discussions. We acknowledge funding from the German Research Foundation (DFG), project KR 48661, and the European Commission H-2020 programme under grant agreement No. 720964. AVK further acknowledges the Academy of Finland for the support under Project No. 286279. The computational support from the HZDR computing cluster is gratefully appreciated.

References

(1) Nastasi, M.; Mayer, J.; Hirvonen, J. *Ion-Solid Interactions - Fundamentals and Applications*; Cambridge University Press, 1996.

(2) Bernas, H., Ed. *Materials Science with Ion Beams*; Springer, 2010.

(3) Archanjo, B. S.; Barboza, A. P. M.; Neves, B. R. A.; Malard, L. M.; Ferreira, E. H. M.; Brant, J. C.; Alves, E. S.; Plentz, F.; Carozo, V.; Fragneaud, B.; MacIel, I. O.; Almeida, C. M.; Jorio, A.; Achete, C. A. The use of a Ga^{+} focused ion beam to modify graphene for device applications. *Nanotechnology* **2012**, *23*, 255305.

(4) Lemme, M. C.; Bell, D. C.; Williams, J. R.; Stern, L. A.; Baugher, B. W. H.; Jarillo-Herrero, P.; Marcus, C. M. Etching of Graphene Devices with a Helium Ion Beam. *ACS Nano* **2009**, *3*, 2674–2676.

(5) Kalhor, N.; Boden, S. A.; Mizuta, H. Sub-10 nm patterning by focused He-ion beam milling for fabrication of downscaled graphene nano devices. *Microelectronic Engineering* **2014**, *114*, 70–77.

(6) Bell, D. C.; Lemme, M. C.; Stern, L. A.; Williams, J. R.; Marcus, C. M. Precision cutting and patterning of graphene with helium ions. *Nanotechnology* **2009**, *20*, 455301.

(7) Standop, S.; Lehtinen, O.; Herbig, C.; Lewes-Malandrakis, G.; Craes, F.; Kotakoski, J.; Michely, T.; Krasheninnikov, A. V.; Busse, C. Ion impacts on graphene/Ir(111): interface channeling, vacancy funnels, and a nanomesh. *Nano Letters* **2013**, *13*, 1948–55.

(8) Madauss, L.; Ochedowski, O.; Lebius, H.; Ban-dEtat, B.; Naylor, C. H.; Johnson, A. T. C.; Kotakoski, J.; Schleberger, M. Defect engineering of single- and few-layer MoS_2 by swift heavy ion irradiation. *2D Materials* **2017**, *4*, 015034.

(9) Nanda, G.; Hlawacek, G.; Goswami, S.; Watanabe, K.; Taniguchi, T.; Alkemade, P. F. Electronic transport in helium-ion-beam etched encapsulated graphene nanoribbons. *Carbon N. Y.* **2017**, *119*, 419–425.

(10) Wang, D.; Wang, Y.; Chen, X.; Zhu, Y.; Zhan, K.; Cheng, H.; Wang, X. Layer-by-layer thinning of two-dimensional MoS_2 films by using a focused ion beam. *Nanoscale* **2016**, *8*, 4107–4112.

(11) Stanford, M. G.; Pudasaini, P. R.; Cross, N.; Mahady, K.; Hoffman, A. N.; Mandrus, D. G.; Duscher, G.; Chisholm, M. F.; Rack, P. D. Tungsten Diselenide Patterning and Nanoribbon Formation by Gas-Assisted Focused-Helium-Ion-Beam-Induced Etching. *Small Methods* **2017**, *1*, 1600060.

(12) Bertolazzi, S.; Bonacchi, S.; Nan, G.; Pershin, A.; Beljonne, D.; Samorì, P. Engineering Chemically Active Defects in Monolayer MoS_2 Transistors via Ion-Beam Irradiation and Their Healing via Vapor Deposition of Alkanethiols. *Advanced Materials* **2017**, *29*, 1606760.

(13) Chow, P. K.; Jacobs-Gedrim, R. B.; Gao, J.; Lu, T.-M.; Yu, B.; Terrones, H.; Koratkar, N. Defect-Induced Photoluminescence in Monolayer Semiconducting Transition Metal Dichalcogenides. *ACS Nano* **2015**, *9*, 1520–1527.

(14) Lin, Z.; Carvalho, B. R.; Kahn, E.; Lv, R.; Rao, R.; Terrones, H.; Pimenta, M. A.; Terrones, M. Defect engineering of two-dimensional transition metal dichalcogenides. *2D Materials* **2016**, *3*, 022002.

(15) Fox, D. S. et al. Nanopatterning and Electrical Tuning of MoS_2 Layers with a Subnanometer Helium Ion Beam. *Nano Letters* **2015**, *15*, 5307–5313.

(16) Ma, L.; Tan, Y.; Ghorbani-Asl, M.; Boettger, R.; Kretschmer, S.; Zhou, S.; Huang, Z.; Krasheninnikov, A. V.; Chen, F. Tailoring the optical properties of atomically-thin WS_2 via ion irradiation. *Nanoscale* **2017**, *9*, 11027–11034.

(17) Wei, X.; Wang, M.; Bando, Y.; Golberg, D. Electron-Beam-Induced Substitutional Carbon Doping of Boron Nitride Nanosheets, Nanoribbons, and Nanotubes. *ACS Nano* **2011**, *5*, 2916–2922.

(18) Wang, H.; Wang, Q.; Cheng, Y.; Li, K.; Yao, Y.; Zhang, Q.; Dong, C.; Wang, P.; Schwingenschlögl, U.; Yang, W.; Zhang, X. X. Doping Monolayer Graphene with Single Atom Substitutions. *Nano Lett.* **2012**, *12*, 141–144.

(19) Ma, Q. et al. Controlled argon beam-induced desulfurization of monolayer molybdenum disulfide. *Journal of Physics: Condensed Matter* **2013**, *25*, 252201.

(20) Ma, Q. et al. Postgrowth Tuning of the Bandgap of Single-Layer Molybdenum Disulfide Films by Sulfur/Selenium Exchange. *ACS Nano* **2014**, *8*, 4672–4677.

(21) Li, H.; Daukiya, L.; Haldar, S.; Lindblad, A.; Sanyal, B.; Eriksson, O.; Aubel, D.; Hajjar-Garreau, S.; Simon, L.; Leifer, K. Site-selective local fluorination of graphene induced by focused ion beam irradiation. *Scientific Reports* **2016**, *6*, 19719.

(22) Krasheninnikov, A. V.; Nordlund, K. Ion and electron irradiation-induced effects in nanostructured materials. *J. Appl. Phys.* **2010**, *107*, 071301.

(23) Hlawacek, G.; Veligura, V.; Gastel, R. V.; Poelsema, B.; Hlawacek, G.; Veligura, V.; Gastel, R. V.; Poelsema, B. Helium ion microscopy. *Journal of Vacuum Science & Technology B: Microelectronics and Nanometer Structures* **2014**, *32*, 020801.

(24) Schmidt, M. E.; Iwasaki, T.; Muruganathan, M.; Haque, M.; Ngoc, H. V.; Ogawa, S.; Mizuta, H. Structurally Controlled Large-Area 10 nm Pitch Graphene Nanomesh by Focused Helium Ion Beam Milling. *ACS Applied Materials & Interfaces* **2018**, *10*, 10362–10368.

(25) Iberi, V.; Liang, L.; Ievlev, A. V.; Stanford, M. G.; Lin, M.-W.; Li, X.; Mahjouri-Samani, M.; Jesse, S.; Sumpter, B. G.; Kalinin, S. V.; Joy, D. C.; Xiao, K.; Belianinov, A.; Ovchinnikova, O. S. Nanoforging Single Layer $MoSe_2$ Through Defect Engineering with Focused Helium Ion Beams. *Scientific Reports* **2016**, *6*, 30481.

(26) Nanda, G.; Goswami, S.; Watanabe, K.; Taniguchi, T.; Alkemade, P. F. A. Defect Control and n-Doping of Encapsulated Graphene by Helium-Ion-BeamIrradiation. *Nano Lett.* **2015**, *15*, 4006–4012.

(27) Ghorbani-Asl, M.; Kretschmer, S.; Spearot, D. E.; Krasheninnikov, A. V. Two-dimensional MoS_2 under ion irradiation: from controlled defect production to electronic structure engineering. *2D Materials* **2017**, *4*, 025078.

(28) Lehtinen, O.; Kotakoski, J.; Krasheninnikov, A. V.; Tolvanen, A.; Nordlund, K.; Keinonen, J. Effects of ion bombardment on a two-dimensional target: Atomistic simulations of graphene irradiation. *Phys. Rev. B* **2010**, *81*, 153401.

(29) Yoon, K.; Rahnamoun, A.; Swett, J. L.; Iberi, V.; Cullen, D. A.; Vlassiouk, I. V.; Belianinov, A.; Jesse, S.; Sang, X.; Ovchinnikova, O. S.; Rondinone, A. J.; Unocic, R. R.; van Duin, A. C. Atomistic-Scale Simulations of Defect Formation in Graphene under Noble Gas Ion Irradiation. *ACS Nano* **2016**, *10*, 8376–8384.

(30) Bellido, E. P.; Seminario, J. M. Molecular Dynamics Simulations of Ion-Bombarded Graphene. *Journal of Physical Chemistry C* **2012**, *116*, 4044.

(31) Wang, D.; Li, X. B.; Han, D.; Tian, W. Q.; Sun, H. B. Engineering two-dimensional electronics by semiconductor defects. *Nano Today* **2017**, *16*, 30–45.

(32) Fox, D.; Zhou, Y. B.; O'Neill, A.; Kumar, S.; Wang, J. J.; Coleman, J. N.; Duesberg, G. S.; Donegan, J. F.; Zhang, H. Z. Helium ion microscopy of graphene: Beam damage, image quality and edge contrast. *Nanotechnology* **2013**, *24*, 335702.

(33) Bangert, U.; Pierce, W.; Kepaptsoglou, D. M.; Ramasse, Q.; Zan, R.; Gass, M. H.; Van den Berg, J. A.; Boothroyd, C. B.; Amani, J.; HofsÃd'ss, H. Ion Implantation of GrapheneâĂŤToward IC Compatible Technologies. *Nano Letters* **2013**, *13*, 4902–4907, PMID: 24059439.

(34) Wilhelm, R. A.; Gruber, E.; Schwestka, J.; Kozubek, R.; Madeira, T. I.; Marques, J. P.; Kobus, J.; Krasheninnikov, A. V.; Schleberger, M.; Aumayr, F. Interatomic Coulombic Decay: The Mechanism for Rapid Deexcitation of Hollow Atoms. *Phys. Rev. Lett.* **2017**, *119*, 103401.

(35) Akcöltekin, S.; Bukowska, H.; Peters, T.; Osmani, O.; Monnet, I.; Alzaher, I.; D'Etat, B. B.; Lebius, H.; Schleberger, M. Unzipping and folding of graphene by swift heavy ions. *Applied Physics Letters* **2011**, *98*, 103103.

(36) Naitou, Y.; Iijima, T.; Ogawa, S.; Naitou, Y.; Iijima, T.; Ogawa, S. Direct nano-patterning of graphene with helium ion beams Direct nano-patterning of graphene with helium ion beams. *Applied Physics Letters* **2015**, *106*, 033103.

(37) Wang, B.; Yang, S.; Chen, J.; Mann, C.; Bushmaker, A.; Cronin, S. B. Radiation-induced direct bandgap transition in few-layer MoS_2. *Applied Physics Letters* **2017**, *111*, 131101.

(38) Maguire, P.; Fox, D. S.; Zhou, Y.; Wang, Q.; O'Brien, M.; Jadwiszczak, J.; Cullen, C. P.; McManus, J.; McEvoy, N.; Duesberg, G. S.; Zhang, H. Defect Sizing, Separation and Substrate Effects in Ion-Irradiated Monolayer 2D Materials. *ArXiv:1707.08893* **2017**,

(39) Kalbac, M.; Lehtinen, O.; Krasheninnikov, A. V.; Keinonen, J. Ion-Irradiation-Induced Defects in Isotopically-Labeled Two Layered Graphene: Enhanced In-Situ Annealing of the Damage. *Adv. Mater.* **2013**, *25*, 1004–1009.

(40) Li, W.; Wang, X.; Zhang, X.; Zhao, S.; Duan, H.; Xue, J. Mechanism of the Defect Formation in Supported Graphene by Energetic Heavy Ion Irradiation: the Substrate Effect. *Scientific Reports* **2015**, *5*, 9935.

(41) Guo, B.; Liu, Q.; Chen, E.; Zhu, H.; Fang, L.; Gong, J. R. Controllable N-doping of graphene. *Nano Letters* **2010**, *10*, 4975–4980.

(42) Buchowicz, G.; Stone, P. R.; Robinson, J. T.; Cress, C. D.; Beeman, J. W.; Dubon, O. D. Correlation between structure and electrical transport in ion-irradiated graphene grown on Cu foils. *Applied Physics Letters* **2011**, *98*, 032102.

(43) Plimpton, S. Fast Parallel Algorithms for Short-Range Molecular Dynamics. *Journal of Computational Physics* **1995**, *117*, 1 – 19.

(44) Jiang, J.-w.; Park, H. S.; Rabczuk, T. Molecular dynamics simulations of single-layer molybdenum disulphide and thermal conductivity. *Journal of Applied Physics* **2013**, *114*, 064307.

(45) Ziegler, J. F.; Biersack, J. P.; Ziegler, M. D. *SRIM - The Stopping and Range of Ions in Matter*; MA: Springer, 1985; pp 93–129.

(46) Wehling, T. O.; Katsnelson, M. I.; Lichtenstein, A. I. Impurities on graphene: Midgap states and migration barriers. *Phys. Rev. B* **2009**, *80*, 085428.

(47) Lin, Y.-C.; Dumcenco, D. O.; Komsa, H.-P.; Niimi, Y.; Krasheninnikov, A. V.; Huang, Y.-S.; Suenaga, K. Properties of individual dopant atoms in single-layer MoS_2: atomic structure, migration, and enhanced reactivity. *Advanced materials* **2014**, *26*, 2857–61.

(48) Dolui, K.; Rungger, I.; Sanvito, S. Origin of the n-type and p-type conductivity of MoS_2 monolayers on a SiO_2 substrate. *Phys. Rev. B* **2013**, *87*, 165402.

(49) Ziegler, J. F.; Ziegler, M. D.; Biersack, J. P. SRIM - The stopping and range of ions in matter (2010). *Nuclear Instruments and Methods in Physics Research, Section B: Beam Interactions with Materials and Atoms* **2010**, *268*, 1818–1823.

Supplemental Material

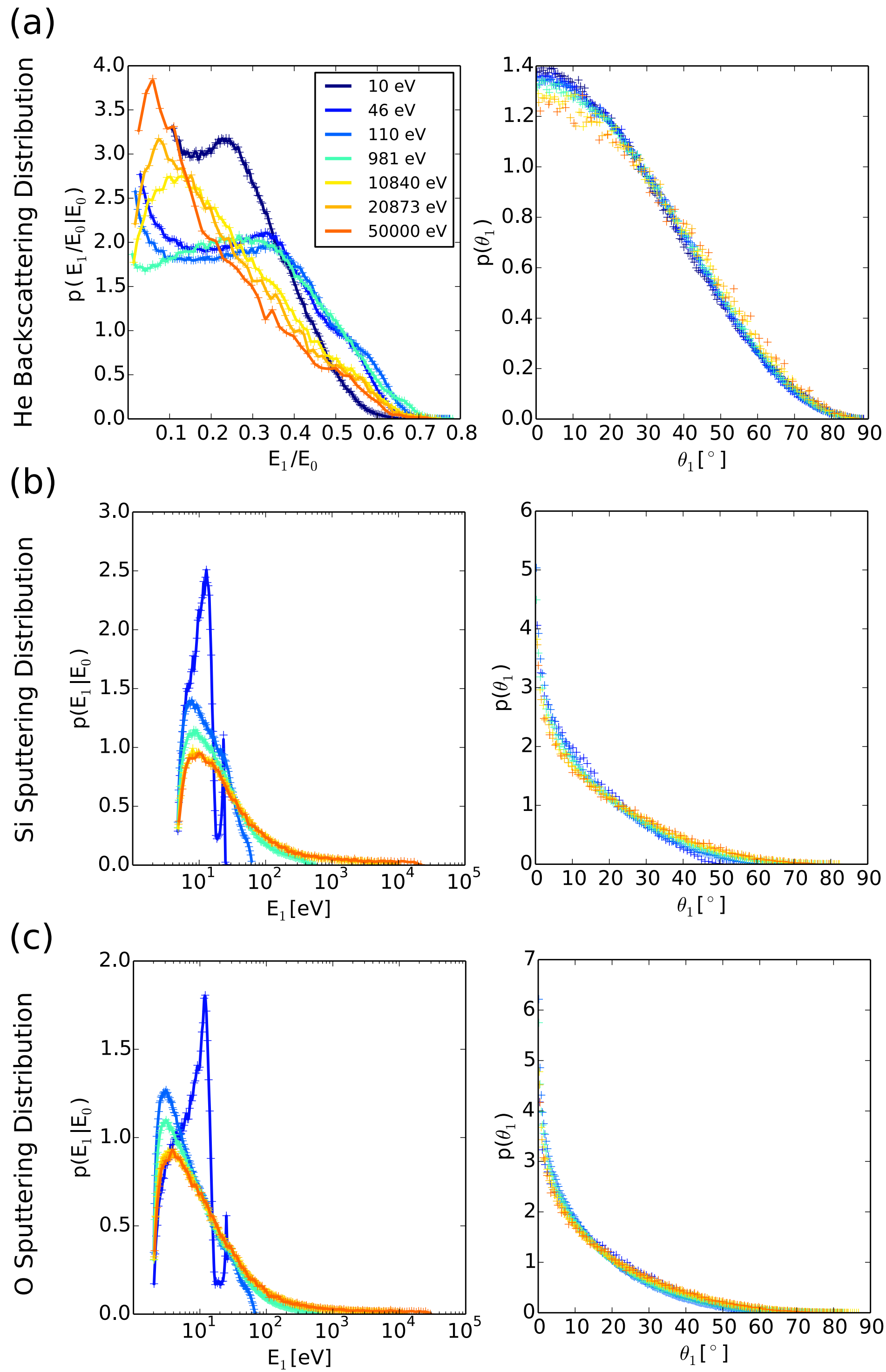

Figure 10: Distribution functions for backscattering/sputtering energy E_1 and angle θ_1 for He, Si and O recoils (from SRIM simulation). The relative backscattering energy distribution $p(E_1/E_0|E_0)$ for the He ion (a) slightly depends on the incident energy E_0 while the sputtering energy distribution $p(E_1|E_0)$ for Si and O (c,b) show a pronounced dependence on it. The angular distribution appears to be independent of the incident ion energy. The backscattering angle distribution for the helium ion can be nicely approximated by $\cos^2\theta_1$

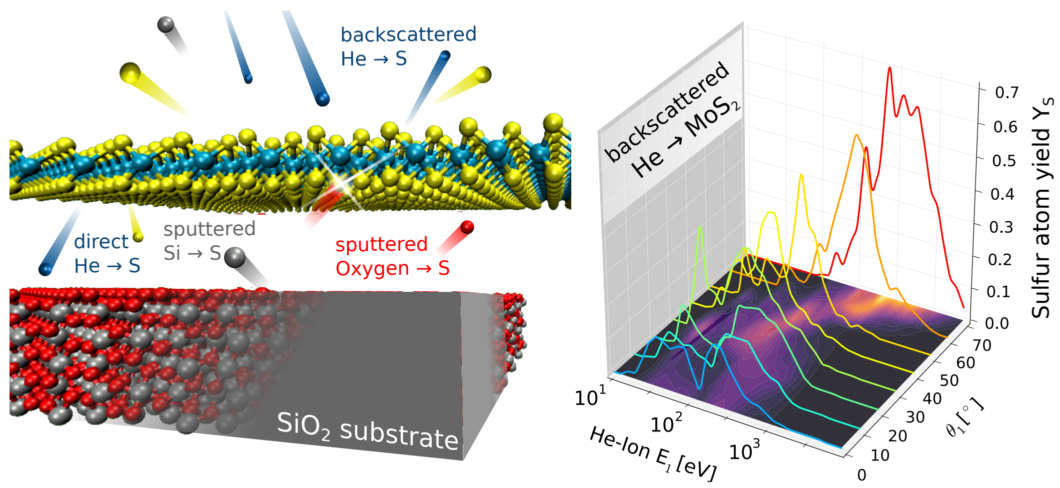

Figure 11: TOC